DIFFRACTION OF AN OBLIQUE COMPRESSION SHOCK IN THE NEIGHBORHOOD OF AN EXTERNAL RIGHT ANGLE

A. I. Maksimov

UDC 533.6.011:532.526.5

Elevation of the requirements to perfect the aerodynamic shapes of flying vehicles evokes the necessity for detailed investigations of the interference between individual structure elements. The angular configurations simulating the site of the fuselage connection to the wing or tail as well as plane air intakes and box-like motor gondolas with lifting surface are among those often encountered.

The supersonic flow around an interior dihedral angle is characterized by primarily the interference between compression shocks and their interaction with boundary layers [1-7], and the exterior angle by flow separation at the edge and the formation of a stalling vortex above the face with lower pressure [8, 9]. The flow near a combination of exterior and interior right angles is complicated by the interaction of complex spatial separation flows with each other and with the compression shocks [10].

Experimental investigations of supersonic longitudinal flow around an exterior right angle with incidence of an external oblique compression shock and without it were performed in the T-313 wind tunnel of the Institute of Theoretical and Applied Mechanics of the Siberian Branch, Academy of Sciences of the USSR is a range of angles of attack from $-4°$ to $20°$, at the Mach number $M_\infty = 2.27$ and the Reynolds number $Re \approx 27 \cdot 10^6$ (per 1 m characteristic dimension). The errors in the true values of the angles of attack α did not exceed $\pm 0.05°$.

The model of the angular configuration (Fig. 1) 400 mm long and 175 and 90 mm, respectively, for the width of the upper and side faces along the leading edge, is fastened by a sword-like suspension of the α-mechanism, while a shock generator in the form of a 300 × 300 mm flat plate is mounted on the floor of the tunnel working section; 132 drainage holes are placed in six transverse sections separated from each other by 25 mm, where the first of them is at a distance x = 75 mm from the leading edge of the angle. The pressure distributions were measured by a MID-100 hundred-channel device using an automated "Analog-1" information collecting system [11]. A LG-106M-1 cw argon laser of $\sim$1 W radiation intensity was used for spatial visualization of the flow.

1. For the flow around an isolated exterior right angle with a fixed Mach number the ratio between the pressures on the model faces is $p_u/p_s = \nu$ (p_u is the pressure on the upper, and p_s on the side face) in the case $\alpha > 0$, conversely for $\alpha < 0$, and is determined only by the magnitude of the angle of attack of the angular configuration α_a. When α_a is zero, $\nu = 1$ and the limit streamlines (LSL) on the model surface are parallel to the edge of the angular configuration and an almost uniform pressure distribution is observed in all sections (Fig. 2).

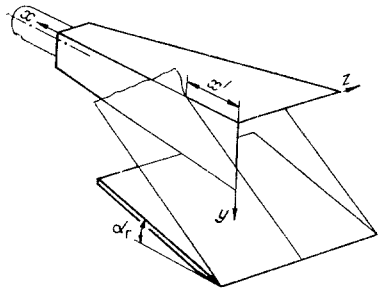

Fig. 1

Novosibirsk. Translated from Zhurnal Prikladnoi Mekhaniki i Tekhnicheskoi Fiziki, No. 4, pp. 146-156, July-August, 1987. Original article submitted June 18, 1986.

 0021-8944/87/2804-0608$12.50

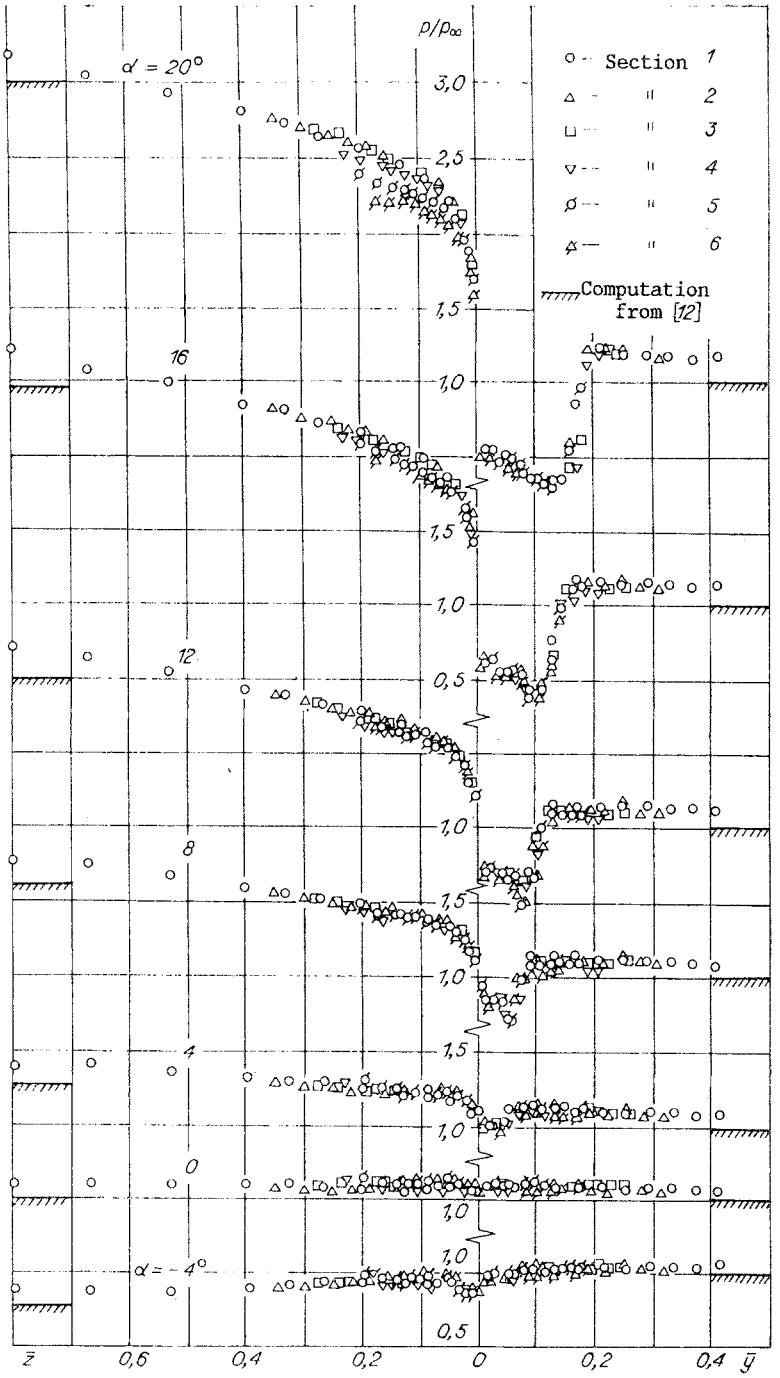

Fig. 2

Here all six transverse sections are combined together by using the conical coordinates $\bar{z} = z/x$ and $\bar{y} = y/x$, where x is the longitudinal coordinate of a section, z and y are transverse coordinates of the drainage holes on the surfaces of the upper and side faces of the angle, and p_∞ is the static unperturbed stream pressure.

The negative α_a stream stall at the edge of the exterior angle (diffraction edge) results in the formation of a vortex system above the upper face, and above the side face in the range of positive angles of attack. As ν increases, the single vortex flow pattern is reconstructed into a multivortex and the pattern of the pressure distribution in the zone of vortex influence on the side face is noticeably complicated (Fig. 2). For $\alpha_a = 8°$ ($\nu = 1.6$) criteria for the pressure of an additional vortex II associated with the secondary separation S_2 and the stream attachment along the line R_2 appear clearly, and for $\alpha_a = 16$ and 20° a three-vortex flow scheme is most probably realized (Fig. 3, $\alpha_a = 20°$).

As is seen from Fig. 2, for all values of α the pressure distribution in the sections is stacked in one curve, which confirms the conical nature of the flow in the zone under

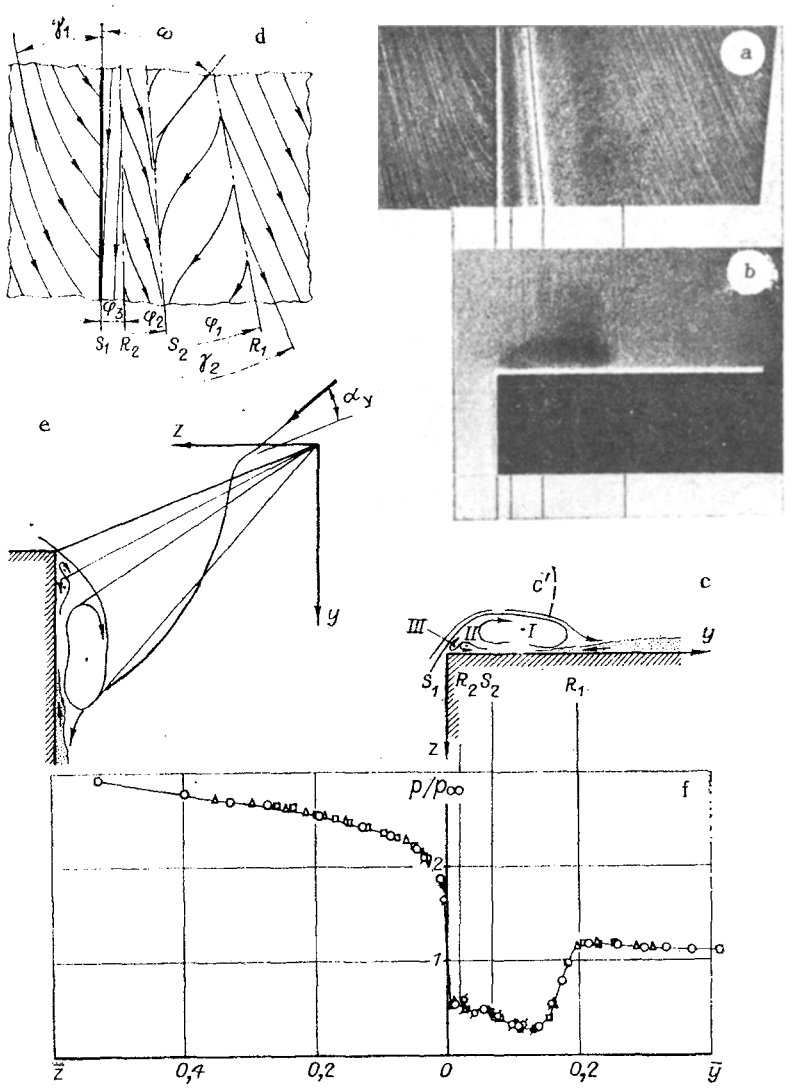

Fig. 3

investigation. Stratification of the curves in the later section on the upper face for $\alpha_a \geq 16°$ is explained by the influence of tip effects. Presented in this same figure as well as in Table 1 are the pressure ratios p/p_∞ as a function of the angles of attack of the model faces, calculated from relationship for an oblique compression shock (for $\alpha > 0$) or Prandtl–Mayer flow ($\alpha < 0$) [12]. Moreover, Table 1 gives computed values of M_α above the upper face, the angles of oblique compression shock deviation φ relative to the surface of this face, and pressure ratios ν on the faces. The pressure values on the upper face surfaces obtained in experiment beyond the limits of the zone of influence of diffraction are somewhat above the computed values both because of the influence of the boundary layer displacement thickness at the true angles of attack and also because of the nonuniformity of the flow field in the working part and the possible deformation of the face under the action of the aerodynamic load.

In direct proximity to the diffraction edge quite significant negative pressure gradients occur because of stream stall. Strong stream rarefaction is observed on the side face surface for $\alpha_a > 0$ under the vortex system. On the boundary of stalling vortex influence, in approximate agreement with the spreading lines for the limit streamlines R_1 (Fig. 3f), the pressure increases until correspondence with the pressure p_∞ for the local M_d near the side face surface (including the influence of the boundary layer displacement thickness). It should be noted that upon diffraction of the bow compression shock W_a on the edge of the angular configuration, the value of M_d increases from M_α to M_∞. Near the spreading line R_1 $M_d < M_\infty$ and therefore, $p_d > p_\infty$, as is actually observed (see Fig. 2).

Photographs of the "laser knife" show that as α_a increases, the core of the main stalling vortex goes over from an initially almost circular shape to an oval, then to a bean shape and

TABLE 1

α°	p_α/p_∞	M_α	φ°	ν
−4	0,773	2,44	—	1,29
0	1	2,27	26,14	1
1	1,063	2,23	25,89	1,06
2	1,130	2,19	25,66	1,13
3	1,199	2,15	25,46	1,20
4	1,272	2,12	25,28	1,27
6	1,429	2,04	25,00	1,43
8	1,600	1,96	24,82	1,60
12	1,990	1,81	24,78	1,99
16	2,452	1,64	25,29	2,45
20	3,004	1,46	26,56	3,00

TABLE 2

α°	$\bar{z}$ or $\bar{\eta}$		$(p/p_\infty)_{min}$	Δ
	p_{max}	p_{min}		
−4	0,05	0,02	0,85	−0,11
0	—	—	—	0
2	0,03	0,015	1,05	−0,05
4	0,05	0,025	0,98	−0,12
8	0,09	0,055	0,72	−0,38
12	0,13	0,08	0,50	−0,60
16	0,16	0,10	0,37	−0,75
20	0,20	0,12	0,30	−0,85

is squeezed to the model surface, while the secondary stream separations have quite small dimensions in thickness (the order of the local boundary layer thickness outside the zone of influence of the vortex system).

For sufficient pressure drops between the upper and side faces the transverse velocity component goes over from the subsonic to the supersonic. In this case, a hanging spatial compression shock c' (Figs. 3b to c) occur above the cores of the stalling vortex.

Outside the diffraction zone, the transverse velocity component is close or equal to zero, is variable within the zone and its maximal value depends on the pressure ratio ν. For conically supersonic flow the reverse passage to the subsonic mode is realized through the normal compression shock as is indeed seen on the photographs for $\alpha_a \geq 16°$. The value of the total velocity vector of those gas particles that run off the upper face and move above the vortex core along a complex spiral line, increases from M_α to M_∞ (Fig. 3e).

In the case of two-dimensional flow separation the spreading line of an oil–soot mixture is ordinarily identified with the line of stream attachment. The validity of such an assumption is verified by the significant pressure rise near the spreading line. In three-dimensional flows the spreading line does not absolutely correspond to stream attachment to the wall [7]. In the case under consideration the spreading line R_1 is formed because of the secondary flow in the boundary layer towards the strong negative pressure gradients observed under the core of the stalling vortex. The gas jets enveloping the vortex system from above continue their motion downstream above the boundary layer and do not attach to the side face surface. Favoring such an assumption is the absence of a noticeable pressure rise near the spreading line R_1 (see Figs. 2 and 3).

Comparison of the visualization pattern and the pressure distribution curves (see Fig. 3) shows that the least value of p/p_∞ corresponds to the approximate position of the center of the main vortex I. Local pressure minima and maxima in the zone of vortex system location are caused by local secondary stream separations and attachments, i.e., by the vortices II and III.

Given in Table 2 are the conical coordinates of the outer boundary of the vortex system and the minimum pressure point under the vortex core I obtained from pressure distribution measurements, the minimal values of the p/p_∞ ratio, and the values $\Delta = (p_{min} - p_b)/p_\infty$ characterizing the vortex system more correctly, where $p_b \approx p_d$ is the background pressure on the surfaces of the upper (for $\alpha_a < 0$) or side ($\alpha_a > 0$) faces of the model outside the zone of influence of the vortex system.

TABLE 3

α	φ_1	φ_2	φ_3	γ_1	γ_{1max}	γ_2	ω
1	2	—	—	2,7	8	1,8	3
2	2,8	—	—	5,2	12	3,3	5,7
3	3,5	0,7	—	7,0	16	4,2	11
4	4,2	1,4	—	8,8	19	5,0	15
6	5,0	1,8	0,8	11,0	25	7,4	22,5
8	5,8	2,2	1,0	12,2	34	8,5	27,5
12	7,5	3,5	1,2	15,8	40	13	35
16	10,0	5,1	1,3	18,2	45	18	42
20	11,5	4,2	1,3	19	45	22	45

Indicated in Table 3 are the angles of deviation of the separation and attachment lines as well as the characteristic limit streamlines in the domain being investigated (the angle notation is given in Fig. 3d), where γ_{1max} is the value of the angle γ_1 in direct proximity to the diffraction edge.

2. The diffraction of an oblique compression shock incident from outside by the edge of the exterior right angle for zero angle α_a was investigated from the shock intensities ξ = 1.27; 1.60; 1.99 and 2.45. According to the computation, the shock reaches the diffraction edge at a distance x' = 100 mm from the leading edge (see Fig. 1).

In this slip flow mode the oblique compression shock W_Γ normal to the side face surface (its projection is shown by dashes in Fig. 4a), interacts with the laminar boundary layer near the leading edge and for ξ = 1.27 (the angle of attack of the compression shock generator is $\alpha_\Gamma = 4°$) causes its separation. With displacement downstream, interaction of this same shock with the boundary layer starts in the transition domain and at approximately ξ = 1.6 ($\alpha_\Gamma = 8°$) a characteristic S-shaped runoff line of the oil–soot mixture associated with the separation appears on the side face surface. As ξ increase further the separation flow zone is broadened significantly and a secondary stream separation line S_2 appears (Fig. 4a, α_Γ = 16°) [4]. The λ-configuration of the shock interacting with the boundary layer occurs on the "laser knife" photographs above the darkened separated flow zone.

Downstream the compression shock and the separation flow it causes gradually approach the edge of the exterior right angle. Initially the leading leg of the λ-shock diffracts and a small vortex flow zone appears above the upper face near the edge of the angular configuration (Figs. 4b and e). The diffracting shock front here acquires the shape of a semicircle in the transverse section with the core of the vortex being forced at the center. Furthermore, diffraction of the trailing leg of the λ-shock starts, the vortex system is strengthened noticeably (Figs. 4c and f), acquires practically circular shape and rises a little above the model surface (Figs. 4d and g).

Because of the appearance of the λ-configuration of the shock, the vortex formation above the upper face starts somewhat earlier than the separation flow zone reaches the edge of the exterior right angle. Diffraction of the leading leg of the λ shock results in deflection of the LSL on the upper face surface from the exterior angle edge. Somewhat downstream the boundary layer separation line S_1 intersects the diffraction edge and merges with the secondary separation line S_3 on the upper face (Fig. 4a).

The pressure drop between the model faces is the reason for the vortex formation above the upper face, as in the case of the flow around an isolated exterior angle. If the pressure drop has been formed earlier because of stream compression above the upper face for $\alpha_a > 0$, then in this case it is an incident compression shock. Although the computed pressure ratios at equal angles α_a and α_Γ remain identical in both cases, the real drop is significantly lower because of the pressure rise above the upper face in the influence zone of the diffracting shock (Fig. 4a). Consequently, even for $\alpha_\Gamma = 16°$ the vortex system being formed is comparatively simple and associated only with the spreading lines R_3 and the stream separation S_3 on the upper face surface.

In the case under consideration the separation flow appearing on the side face because of shock interaction with the boundary layer indeed exerts significant influence on vortex development. With displacement downstream it is involved in formation of the vortex system by the gas overflowing from the side onto the upper face. The part of the boundary layer

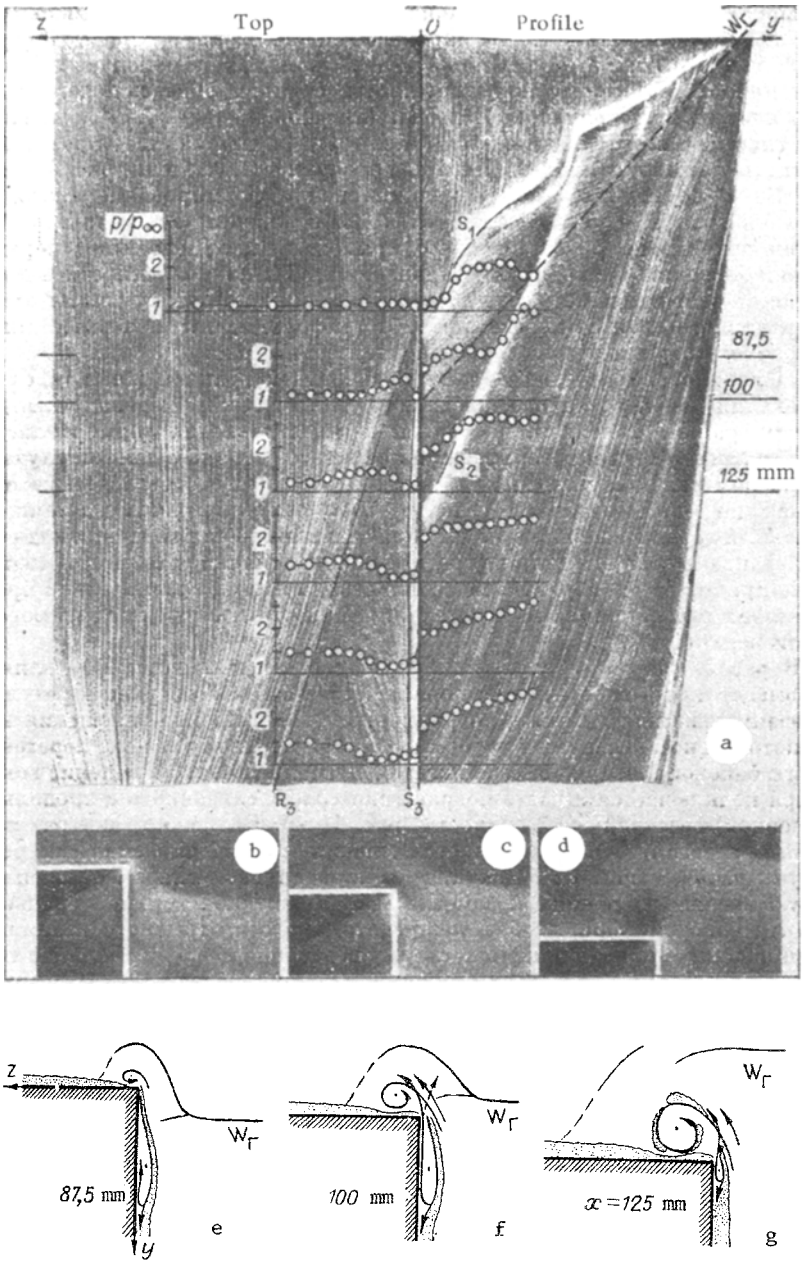

Fig. 4

associated with the longitudinal (main) velocity component (Fig. 4g) is connected in parallel in rotation around the vortex. Again because of such diffraction flow development, in contrast to the flow around an isolated angle, the vortex structure under consideration has a possibly diffuse outer boundary and "floats" noticeably above the upper face.

The pressure distribution on the side face in the preseparation and separation interaction of the shock with the boundary layer corresponds well to the regularities known for such flows. A typical pressure minimum for vortex flow is observed under the vortex core on the upper face (Fig. 4a). However, this minimum does not diminish below the level characteristic for the unperturbed stream, i.e., $\sim p_\infty$ outside the dependence on ξ. Such a situation is apparently associated with the diffraction of the incident shock towards the upper face and the expenditure of part of the stream energy in equalizing the pressure in the vortex location zone.

A noticeable difference in the pressure levels, that increases as the incident compression shock intensity grows, is conserved even at a considerable distance from the leading edge between the upper and side faces. For instance, if an almost identical pressure is observed for $\xi = 1.27$ after diffraction of the shock by the faces ($p/p_\infty \approx 1.25$ in six

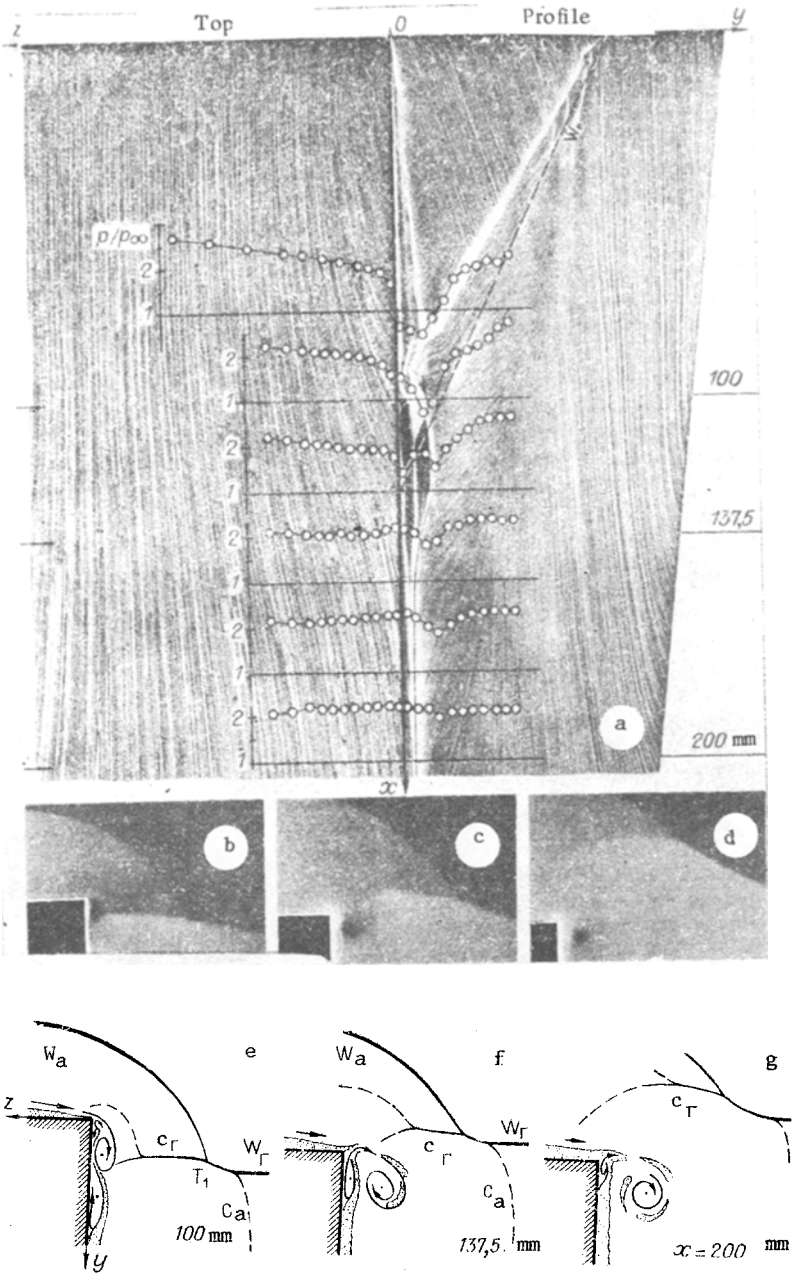

Fig. 5

drainage sections), then for $\xi = 1.6$ the pressure ratios remain at the level 1.3 and 1.55 and for $\xi = 2.45$ at 1.5 and 2.5. It hence also follows that as ξ increases a more significant fraction of the stream energy is expended in the vortex system and diffraction of the shock does not result in a pressure growth adequate to its intensity above the model upper face.

3. The flow around an exterior right angle in the identical angle of attack mode with a compression shock generator (CSG) actually represents the case of unification of the flows considered above. As for independent flow around an angular configuration without a CSG, a flow with stream stall on the edge and vortex system formation is realized in the free diffraction zone in the lading part of the model. The shock W_Γ incident from the generator initially interacts with the diffracting bow shock W_a and then the internal shock c_Γ with the side face boundary layer, with the stalling vortex, and only afterward diffracts across the edge of the angle towards the upper face (Fig. 5, $\alpha_a = \alpha_\Gamma = 16°$, x' = 125 mm). The most important feature of this flow mode is interference of the shock c_Γ with the vortex system near the diffraction edge.

Analogously to the case around a plate with a longitudinal step for a slip angle $\beta = 0$ and $\alpha > 0$ [10], the shock W_a diffracts towards the side face almost along the arc of a

circle in the leading part of the model and, weakening gradually, reaches W_Γ at the point T_1 (Fig. 5, b and e). It then falls into the stream compression zone with $M_\alpha < M_\infty$ and smoothly changes the angle of its deflection relative to the side face surface (until agreement with M_α). For large angles of attack, M_α is considerably less than M_∞ (see Table 1) and a change in the position of the internal shock c_a at the point T_1 is jumplike in nature. If the intensity of the diffracting shock W_a is sufficient, then the incident shock W_Γ (whose continuation is the shock c_Γ) also changes it position noticeably and deviates towards the diffraction edge up to agreement with the local stream parameters for M_d.

Because of the appearance of sweepback of the leading edge at the side face for $\alpha_y \neq 0$ which contributes to acceleration of the laminar transition into a turbulent boundary layer [13], the internal shock c_Γ interacts with the turbulent boundary layer over practically the whole extent of the face, as our oil–soot photographs indicate. If a preseparation flow is observed up to $\alpha = 8°$, with the exception of a small section of the laminar boundary layer at the leading edge, then from $\alpha \geq 12°$ on the side face stream separation is explicitly detected.

As it moves along the model the shock c_Γ reaches the vortex system, its leading and trailing λ legs start to interact with the core of the stall vortex and diffract successively towards the upper face (Figs. 5b, e and c, f). In contrast to the diffraction mode for $\alpha_a = 0$ (Sec. 2), the shock c_Γ is incident in the zone of comparatively high pressure above the upper face and dissipates sufficiently rapidly, becoming visible on the "laser knife" photographs.

Starting from $\alpha = 12°$, numerous stream separation and attachment lines occur in the shock interaction with the vortex zone on the side face and for $\alpha \geq 16°$ (Fig. 5a) still local stagnation sections which lose their clear contours on the oil–soot photographs during wind tunnel stoppage.

For small α the second stream separation line associated with the formation of the vortex system in the free diffraction zone is forced back towards the edge after the action of the shock and gradually merges with it. At angles $\alpha > 12°$ the secondary stream separation line under the vortex and the line of boundary layer separation from the shock c_Γ below the section of intensive mixing of the separation flows under consideration connect together and are carried downstream somewhat remote from the diffraction edge (Fig. 5a).

An increase in α results in magnification of the pressure gradients and complication of the pressure distribution pattern in the domain of shock interference with the vortex system. For $\alpha \leq 12°$ at a distance of $x \approx 2x'$ the pressures on the upper and side face surfaces are equalized and take on a value close to the computed value in conformity with $\alpha_a = \alpha_\Gamma$. Furthermore, as α grows the experimental and computed data do not agree, which is related to the discharge of part of the stream energy into interaction with the vortex and the influence of tip effects (Fig. 6, the z–y axis scale must be doubled).

A partial collision of the streams with the substantially different motion directions occurs during shock and boundary layer separation flow interaction with the vortex system. Because of the nonsymmetric action of the shock c_Γ from above (from the right) and the boundary layer separations from below (from the left), a core of the stall vortex of irregular shape (for large α) starts, in addition to the rotation of the gas with in it, to revolve itself and seem to "tumble" (Fig. 5c and f). As in the preceding case (Sec. 2), the gas from the boundary layer separation zone is involved in rotation around the core by the stream overflowing from the upper onto the side face. As the flow develops further, the low-energy "portion" of the separation flow (because of the transverse velocity component) and the boundary layer that is involved in the rotation dissipate comparatively rapidly into the surrounding high-energy (because of the longitudinal velocity component) stream. The core of the vortex standing off in the external stream is gradually stabilized and acquires a clear circular shape, i.e., is transformed into a cylindrical or conical vortex filament (Figs. 5d and g).

Tests were conducted in three incident shock locations (x' = 100, 125, and 150 mm) to study the nature of the interference between compression shocks of identical intensity and vortex systems of different magnitude for $\alpha_a = \alpha_\Gamma = 8$ and 16°. It turns out that only the scales of the phenomena being investigated (local stream separation, stagnation zones, etc.) vary here. Pressure distributions in the comparable transverse sections 2, 3, 4 and 3, 4, 5 were compared as an illustration in Fig. 7. At the angle $\alpha = 8°$ the data for all three shock locations and the whole possible set of comparable sections are in good agreement (with the

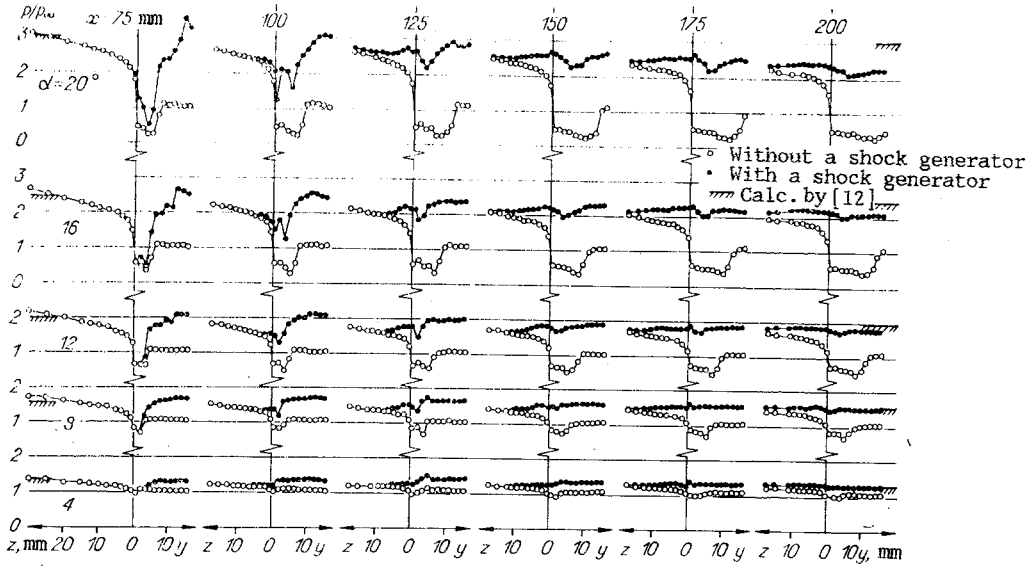

Fig. 6

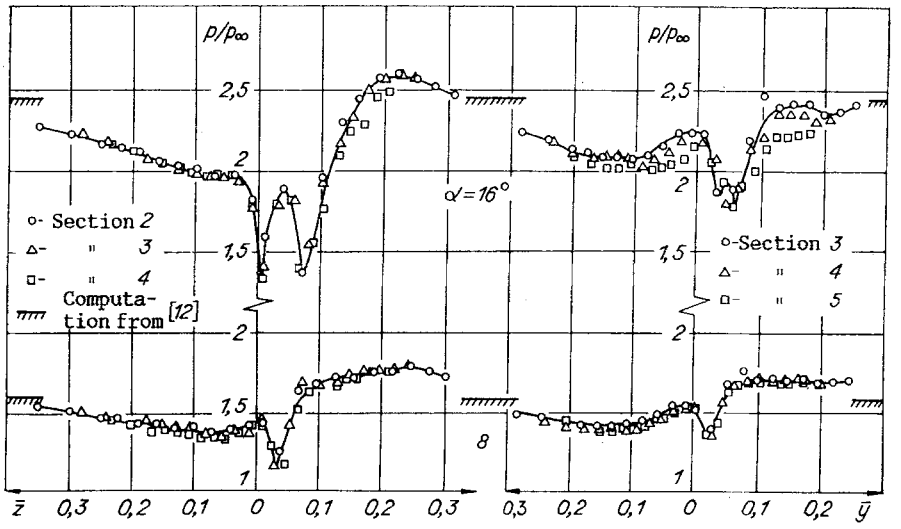

Fig. 7

exception of cases of boundary layer thickness influence in the first three sections on the side face). For $\alpha = 16°$ because of the growth in the intensity of the interacting compression shocks, the vortex formations, etc., more significant pressure gradients are observed, the spread in the data is somewhat greater and equalization of the flow field occurs much more slowly.

Therefore, in a supersonic longitudinal flow around an exterior right angle the increase in the pressure drop between the model faces results in a significant flow complication near the diffraction edge and in the appearance of a spatial hanging compression shock above the core of the main stall vortex. For a model zero angle of attack the diffraction of the oblique compression shock incident on the side face from outide is accompanied by the formation of a vortex system and a pressure rise above the upper face. The principal feature of the flow around an angular configuration in the mode $\alpha_a = \alpha_\Gamma$ is the intensive interaction between the incident shock and the vortex system resulting in the appearance of a free vortex filament that is propagated far downstream up to total dissipation because of the action of viscosity forces.

Interaction between a compression shock and a boundary layer and vortex systems of identical intensity but different size is of the same nature, as is confirmed by both the stream visualization photographs obtained and by pressure distribution measurements on the model surface.

The author is very grateful to A. M. Kharitonov, M. D. Brodetskii, A. A. Zheltovodov and N. F. Vorob'ev for valuable remarks during discussions of the research, and to A. A. Palov for direct participation in the stream visualization experiments by the "laser knife" method.

LITERATURE CITED

1. V S. Dem'yanenko, "Experimental investigation of the spatial supersonic gas flow in the interference domain of intersecting surfaces," Izv. Akad. Nauk SSSR, Mekh. Zhidk. Gaza, No. 6 (1975).
2. V. S. Dem'yanenko and V. A. Igumnov, "Spatial interaction of a shock with a turbulent boundary layer in the interference domain of intersecting surfaces," Izv. Sib. Otd. Akad. Nauk SSSR, Ser. Tekh. Nauk, No. 2 (1975).
3. A. A. Zheltovodov, "Physical features and certain properties of two- and three-dimensional separation flows at supersonic speeds," Izv. Akad. Nauk SSSR, Mekh. Zhidk.Gaza, No. 3 (1979).
4. A. A. Zheltovodov, "Modes and properties of spatial separation flows initiated by oblique compression shocks," Zh. Prikl. Mekh. Tekh. Fiz., No. 3 (1982).
5. M. A. Zubin and N. A. Ostapenko, "Flow structure in the separation domain during interaction of a normal compression shock with the boundary layer in a corner," Izv. Akad. Nauk SSSR, Mekh. Zhidk. Gaza, No. 3 (1979).
6. K. K. Kostyuk, N. A. Blagoveshchenskii, et al., "Experimental investigation of the flow around a dihedral angle and simplest configurations of the triangular plate + conical body type at a high supersonic speed," Tr. TsAGI, No. 2224 (1984).
7. H. Kubota and J. L. Stollery, "An experimental study of the interaction between a glancing shock wave and a turbulent boundary layer," J. Fluid Mech., 116 (1982).
8. V. S. Dem'yanenko and V. P. Fedosov, "Supersonic flow around a convex dihedral angle," Izv. Sib. Otd. Akad. Nauk SSSR, Ser. Tekh. Nauk, No. 3 (1975).
9. G. I. Maikapar and A. I. Pyatnova, "Supersonic flow around the external angle of an air intake shell," Uchen. Zap. TsAGI, 11, No. 3 (1980).
10. M. D. Brodetskii, A. I. Maksimov, and A. M. Kharitonov, "Interaction features of interference and diffraction flows at supersonic speeds," Zh. Prikl. Mekh. Tekh. Fiz., No. 1 (1986).
11. M. A. Amelina, M. D. Brodetskii, et al., "Multichannel pressure meter MID-100," Methods and Techniques of Aerophysical Investigations [in Russian], ITPM, Sib. Otd. Akad. Nauk SSSR, Novosibirsk (1978).
12. G. N. Abramovich, Applied Gas Dynamics [in Russian], Nauka, Moscow (1969).
13. S. V. Kalinina and V. I. Kornilov, "Influence of the sweepback angle and single Reynolds number on boundary-layer transition at supersonic speeds," Zh. Prikl. Mekh. Tekh. Fiz., No. 1 (1973).